Sample title

Electronic state influence on selective bond breaking of core-excited nitrosyl chloride (ClNO)

Peter Salén,[1] Luca Schio,[2] Robert Richter,[3] Michele Alagia,[2] Stefano Stranges,[4,2] Stefano Falcinelli,[5] and Vitali Zhaunerchyk[6]

[1)]*FREIA Laboratory, Department of Physics and Astronomy, Uppsala University, 751 20 Uppsala, Sweden*

[2)]*IOM-CNR Tasc, SS-14, Km 163.5 Area Science Park, Basovizza, I-34149 Trieste, Italy*

[3)]*Elettra - Sincrotrone Trieste, Area Science Park, 34149 Basovizza, Trieste, Italy*

[4)]*Dipartimento di Chimica e Tecnologie del Farmaco, Universitá Sapienza, Roma, I-00185 Italy*

[5)]*Department of Civil and Environmental Engineering, University of Perugia, Via G. Duranti 93, 06125 Perugia, Italy*

[6)]*Department of Physics, University of Gothenburg, 412 96 Gothenburg, Sweden*

(*Electronic mail: vitali.zhaunerchyk@physics.gu.se)

(*Electronic mail: peter.salen@physics.uu.se)

(Dated: 25 August 2022)

The potential for selective bond breaking of a small molecule was investigated with electron-spectroscopy and electron-ion coincidence experiments on ClNO. The electron spectra were measured upon direct valence photo-ionization and upon resonant core-excitation at the N 1*s*- and O 1*s*-edges followed by emission of resonant Auger (RA) electrons. The RA spectra were analyzed with particular emphasis on the assignment of the participator and spectator states. The latter are of special relevance for investigations of how distinct electronic configurations influence selective bond breaking. The electron-ion coincidence measurements provided branching fractions of the produced ion-fragments as a function of electron binding energy. It explicitly demonstrates the influence of the final electronic states created after the photo-ionization and RA decay, on the fragmentation. In particular, we observe a significantly different branching fraction for spectator states compared with participator states. The bonds broken for the spectator states are also found to correlate with the anti-bonding character of the spectator-electron orbital.

I. INTRODUCTION

Selective bond breaking in a molecule opens the door to the control of chemical reactions and to molecular structure determination. For example, preferential breaking of specific bonds induced by soft X-rays was recently demonstrated as a tool for determining the protonation site of biomolecules[1]. X-rays have particular potential for specific bond breaking owing to the ability of selectively creating a core-hole at a specific molecular site upon excitation or ionization with suitable photon energy. The localized character of such excitations at a chosen molecular site hints to the possibility of controlled bond breaking and consequently its feasibility has been intensively explored[2–19]. Experimental studies have demonstrated that site-specific bond breaking, i.e., the cleavage of the bonds connected to the core-hole site created by excitation or ionization, can be enhanced in some cases[2–6,8,10,11,13–15,17–19]. However, the effect is often relatively small and is not fully understood. Furthermore, these observations of site-specific bond cleavage are complemented by several examples where the bonds are preferentially broken at sites other than the core excited one[7,9,12].

Selectivity of bond cleavage may depend on several factors including 1) the type of excitation (valence excitation or ionization, core excitation or ionization), 2) the properties of the created electronic states (bound, unbound, charge state), 3) the properties of the molecule (size, structure, constituents).

1) Valence excitation does not involve the formation of a core hole and is not appropriate for site-specific fragmentation studies, although the character of the created electronic state can influence the fragmentation[20]. In contrast, the site-specific nature of the core excitation and core ionization may be conserved in the final state formed after rapid Auger decay. Auger decay resulting from core ionization creates a doubly or multiply charged ion, while resonant Auger (RA) decay succeeding resonant core excitation typically creates a singly charged ion. The higher charge state associated with states formed by normal Auger decay following core-ionization may lead to fast fragmentation through Coulomb explosion, which can benefit site-specific bond breaking because the time for redistribution of excess energy within the molecule, after the localized excitation, is reduced[21].

2) RA decay occurs via a participator or spectator process with conceivably different prospects for selective bond cleavage. In participator decay the core excited electron participates in the Auger process where one electron fills the core hole and one electron is ejected. It produces a 1-hole ($1h$) final state equivalent to that formed by ejecting an electron through direct ionization. In the spectator decay the core excited electron is not involved in the Auger decay and it thus generates a 2-hole 1-particle ($2h-1p$) final state for which the character of the spectator-electron orbital can influence the fragmentation. For example, an electron excitation to an orbital with an antibonding character at a specific bond more likely leads to cleavage of that bond. It is worth pointing out that quite often, because of the configuration interaction, electronic states cannot be solely ascribed as either $1h$ or $2h-1p$ states[22].

3) The influence of the molecular properties on site-specific bond breaking has been investigated by Nagaoka et al.[8] on

the bridged trihalosilyltrimethylsilyl, X_3SiC_n- $H_mSi(CH_3)_3$, where n = 0-2, m = 0-4, and X = F or Cl. They concluded that a significant difference in chemical environment at the two Si sites is advantageous for such site-specific cleavage. Moreover, a longer bridge between the Si sites prevents charge migration and therefore promotes site-specific fragmentation. As will be discussed further below, the molecular size can also be an important factor due to its connection to the rate of excess energy redistribution.

The influence of electronic state populations formed upon the Auger decay on the fragmentation pattern, depends on the excess energy redistribution timescale[23,24] and that of the dissociation[25]. A fast internal conversion (IC) to the electronic ground state and intramolecular vibrational redistribution (IVR) to all vibrational modes, create a thermal molecule that fragments statistically[9,26]. In this case the fragmentation pattern is determined by the molecular excess energy associated with the different Auger states, but is unaffected by their character. The Auger decay tends to be localized around the core-excited site because the Auger rate for a specific final state depends on the overlap of the orbitals involved in the excitation and decay process[27,28]. Elimination of the localization and character of the electronic state formed after Auger decay, by the spread of energy within the molecule, makes the possibilities for selective bond breaking limited. It is therefore critical whether the excess energy is redistributed before the dissociation, or if it is slow enough to allow influence from the Auger electronic states on the fragmentation process.

The redistribution of the parent-ion electronic energy into vibrational energy is typically faster for larger molecules. The reason is that IC and IVR rates relate to the available number of vibrational modes which is proportional to molecular size (more specifically, to number of atoms in a molecule). IC transfers electronic energy into vibrational energy of a lower electronic state, while IVR distributes vibrational energy further into the manifold of vibrational modes. According to Fermi's golden rule[30], the rates of the two processes are proportional to the density of vibrational states. They can both proceed on sub-picosecond timescales and may thus compete with the dissociation dynamics[31,32]. It should be noted, however, that there is a strong dependence of the redistribution rate on the potential-energy surface landscape of the specific molecule[33].

The mechanism behind selective fragmentation can be addressed using ion-electron coincidence experiments[9,10,12,34] because it permits to correlate the produced ions with a specific Auger final state. It therefore provides a tool for understanding the influence of the electronic states on the fragmentation and the related capacity for selective bond rupture. For example, the site- and state-specific fragmentation of 2Br-pyrimidine following RA decay was investigated using this technique[12]. They observed no direct correlation between the excited site and bonds broken but showed that significantly different populations of RA states formed at different core-excitation energies determined the fragmentation pattern. In a related study[9] on photoionized chloro- and bromoacetic acid samples the key role of the molecular internal energy on the fragmentation was emphasized. In our previous investigation of *N*-methyltrifluoroacetamide (FNMA) we observed site-specific fragmentation patterns which could also be explained by the specific RA population associated with a core-excitation[34]. Also in this case, the molecular excess energy distribution generated by Auger decay, i.e., the internal-energy distribution, was found to be the significant parameter and the properties of the electronic states populated did not influence the site-specific dissociation. It shows that site-specific fragmentation can occur for favorable populations of the Auger states also when the memory of the initially formed electronic states is lost through redistribution of energy. Such distributions among the Auger final states can thus be confused with electronic state influence. In the case of FNMA the site-specific bond breaking could be explained by the population of the RA states having a significant weight at excess energies where only a channel favoring such bond cleavage is thermodynamically available. In the described studies[9,12,34] the observed influence of the core hole on the fragmentation, via the nuclear dynamics occurring before Auger decay, was not a significant factor. However, such influence has been reported previously[5,11,13,35].

Fragmentation studies on medium and large sized molecules have shown tendencies of site-specific cleavage[1,3,8,14–16], but also the absence of it[9,12,26,34]. In some cases it can be difficult to determine the reason for the obtained site-specificity, i.e., whether it is caused by the electronic state characters or whether quickly distributed excess-energy favors particular fragmentation channels. However, both explanations may be valid for medium sized molecules since the molecular properties affect both the speed of energy redistribution and fragmentation, thus the potential for site-specific bond breaking is expected to be strongly affected by the properties of the individual molecule. For small molecules signatures of site-specific bond breaking have been observed for example in $ClCH_2Br$[10], HNCO[17], N_2O[18], CO_2[13], O_3[11] and ClNO[19].

In this work we have investigated site- and state-selective fragmentation of nitrosyl chloride, ClNO, upon vacuum-ultraviolet (VUV) ionization and resonant excitation at the N 1*s* and O 1*s*-edges. The core-excited states and dissociation dynamics upon core excitation of the ClNO molecule were already extensively investigated by our research group (Ref.[19] and[36]), providing a solid basis for the study of the Auger decay process. The present study uses electron-ion coincidence measurements, which specifically allow us to investigate the influence of the electronic states formed upon RA on the fragmentation of ClNO. For such a small molecule the electronic state can have a significant effect on the fragmentation based on the potentially slow redistribution of excess energy as discussed above. We have compared it with our previous similar studies of the larger molecule FNMA, for which no signs of such electronic state influence was observed. In contrast, clear evidence of this effect is obtained for ClNO by investigating the correlation between the RA state and the ion branching fractions. In particular, spectator states display a significantly different branching fraction compared with participator states. Moreover, a pronounced correlation between the bond broken and the antibonding character of the spectator-electron orbital

is observed.

II. EXPERIMENTAL AND THEORETICAL METHODS

The experiments were performed at the GasPhase Photoemission beamline of the Elettra synchrotron in Trieste[37]. It provides soft X-rays that can be tuned with respect to photon energy using a variable-gap undulator and a monochromator to permit a spectral width below the natural linewidth. The ClNO gas was prepared as described in Ref.[36] and was injected effusively into the experimental chamber where it intersected the X-ray beam. The Near-Edge X-ray Absorption Fine-Structure (NEXAFS) spectra at the N 1*s*- and O 1*s*-edges of ClNO were obtained by measuring the produced ions when scanning the soft X-ray photon energy. The NEXAFS spectra were calibrated to those previously reported in Ref.[36]. The vacuum-ultraviolet photoelectron spectra (VUV PES) and RA spectra were recorded with a commercial hemispherical electron energy analyzer (VG220i). Residual H_2O, NO (generated by the spontaneous dissociation of ClNO) and N_2 features were used for calibrating the VUV-PES. The RA spectra were subtracted with below-resonance contributions, except for the electron-ion coincidence spectra. The acquisition time, photon flux and gas pressure were used for normalization of the below-resonance subtraction. Ions in coincidence with electrons were measured with a home-built ion time-of-flight spectrometer[38].

Molecular orbitals and thermodynamic thresholds of various dissociation channels were obtained with the Gaussian 16 software[39]. The thresholds were found as difference between enthalpies of dissociation products and parent ClNO molecules. The enthalpies were calculated with the G4 composite method. Molecular orbitals were found for the ClNO geometry optimized at the B3LYP/aug-cc-pTVZ level of theory.

III. RESULTS AND DISCUSSION

A. VUV photoelectron spectra

Figure 1 shows the experimental VUV PES of ClNO (red solid line) measured at the photon energy of 60 eV. The spectrum shows five well distinct features at 11.4 eV, 16.2 eV, 17.2 eV, 19.0 eV, and 22.1 eV. There is also a broad diffuse feature peaked at 23.1 eV. Assignment of the spectral features were reported in Refs.[40,41]. The electronic structure of ClNO is[40]

$$\ldots(10a')^2(11a')^2(2a'')^2(3a'')^2(12a')^2(13a')^2.$$

The peak at 11.4 eV is associated with ionization of $3a''$, $12a'$, and $13a'$ orbitals which are very close in energies. Frost et al.[41] assigned the 16.2 eV, 17.2 eV, and 19.0 eV peaks to electrons ionized from $2a''$, $11a'$, and $10a'$ orbitals, respectively. However, Lacombe et al.[40] using a rigorous multiconfiguration treatment showed that the spectral features above 11.4 eV cannot be assigned solely based on the one-particle model of ionization. The peak assignment by Lacombe et al.[40] is presented in Table I. In particular, they showed that the 16.2 eV peak consists of two satellite lines of another state, while the state with predominantly $(2a'')^{-1}$ configuration contributes to the 17.2 eV peak. Furthermore, according to their calculations, the 17.2 eV peak contains contribution from another state that is superimposed from ionizations of $10a'$ and $11a'$ orbitals.

Although the peak at 22.1 eV was not assigned in either work, we suppose that since this peak is distinct and has a significant intensity it is associated with the state of chiefly $(9a')^{-1}$ configuration. The spectrum above 23 eV does not contain any clear peaks and we believe that it is due to the complete breakdown of the molecular orbital picture of ionization when the intensity of main lines is dispersed over satellite states[42].

Weak structures attributed to residual H_2O (12.6 eV, 13 eV and 14.7 eV)[43], NO (13.8 eV and 16.5 eV)[44–47], and N_2 (15.7 eV)[48], can also be observed as indicated in the figure. Although the feature attributed to NO at 13.8 eV in Fig. 1 is often neglected in studies of the NO electronic structure[45–47], our ClNO VUV PES recorded at different relative densities of ClNO and the residual gases strongly suggests NO as the source. The weak broad band at 14.0-15.4 eV assigned to ionization of water overlaps with the theoretical ionization energies (IEs) of the diexcited $(2h-1p)$ states of ClNO (see Table I) and could also contain weak contributions from such states. The experimental peak positions of the ClNO PES marked with black stars are collected in Table I together with the theoretical IEs.

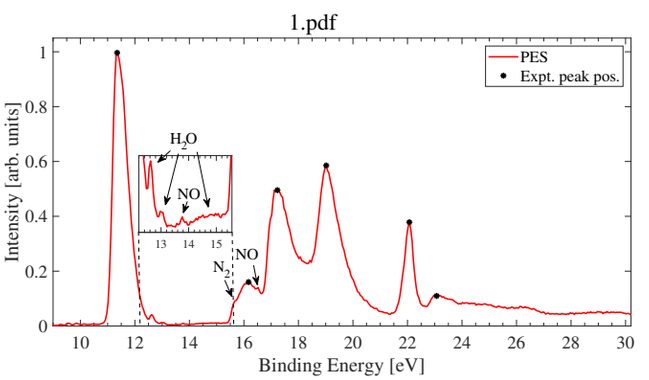

FIG. 1. The VUV PES measured at $h\nu = 60$ eV is presented by the red curve. The black stars indicate estimated experimental peak positions. The arrows mark weak features that originate from residual H_2O, NO and N_2. The inset shows a zoom-in to the low-intensity region of the ClNO PES at 12.2 eV - 15.5 eV, which is dominated by residual H_2O and NO. The experimental energy resolution is ∼200 meV.

B. Resonant Auger spectra

Resonant Auger spectra display contributions primarily from the $1h$ (participator) and $2h-1p$ (spectator) states formed upon resonant core excitation. Figures 2 and 3 (right panels) show the RA spectra upon N 1*s*- and O 1*s*-excitation, respectively. The RA spectra are presented for several pho-

TABLE I. Experimental and calculated[40] ionization energies (IEs) of ClNO. The experimental values are extracted from the VUV PES (Fig. 1) and resonant-Auger (RA) spectra (Fig. 4). Assignments of the peaks associated with the RA processes (Fig. 4) are given in brackets where p denotes participator states, s denotes spectator states and x denotes uncertain attribution. Calculated IEs and cross-sections together with assignments and coefficient of the corresponding configuration in parenthesis are taken from Ref.[40].

Experiment		Theory[40]		
Energy (eV) VUV PES	Energy (eV) RA	Calculated IE (eV)	Assignment	Cross-section (Mbarns)
11.4	11.4 {p1}	10.79	$(13a')^{-1}$ (0.93)	0.095
		11.10	$(12a')^{-1}$ (0.91)	0.032
		11.14	$(3a'')^{-1}$ (0.91)	1.65
	13.0 {x1}			
	14.4 {s1}	14.54	$(13a')^{-1}$ (0.06) + diexcited	0.029
		14.93	$(2a'')^{-1}$ (0.05) + diexcited	0.003
16.2		15.29	$(10a')^{-1}$ (0.18)	0.017
			$(11a')^{-1}$ (-0.18)	
		15.33	$(11a')^{-1}$ (-0.46)	0.084
			$(10a')^{-1}$ (0.20)	
17.2	17.0 {p2}	16.33	$(2a'')^{-1}$ (0.20)	0.004
		16.38	$(10a')^{-1}$ (0.74)	0.106
			$(11a')^{-1}$ (0.36)	
		16.45	$(11a')^{-1}$ (-0.17)	0.016
			$(10a')^{-1}$ (-0.10)	
		16.93	$(2a'')^{-1}$ (0.83)	0.061
		17.46	$(3a'')^{-1}$ (-0.15)	0.014
	18.2 {s2}			
19.0	19.0 {p3}	18.66	$(2a'')^{-1}$ (-0.23)	0.004
		19.92	$(12a')^{-1}$ (0.14)	0.008
		20.56	$(11a')^{-1}$ (0.63)	0.014
			$(10a')^{-1}$ (-0.25)	
	19.7 {x2}			
	20.0 {s3}			
	20.1 {x3}			
	21.1 {s4}			
	21.4 {s5}			
22.1	22.5 {p4}			
23.1	23.5 {p5}			
	26.9 {s6}			
	28.8 {s7}			

ton energies, which are indicated in the NEXAFS spectrum in the left panels. The NEXAFS spectra were previously investigated in more detail in Ref.[36] and the two peaks in both NEXAFS spectra were assigned to excitation of the 1s electron from the respective atom to LUMO and LUMO+1 orbitals. The LUMO and LUMO+1 orbitals of the excited molecule are visualized in Ref.[36]. In Fig. 4, the RA spectra recorded at resonances for the N 1s- and O 1s-edges are placed in the same figure for direct comparison, together with the VUV PES. Direct-ionization background signals (blue dashed line in Figs. 2 and 3) have been removed in Figs. 2-4, in order to highlight the resonant parts.

Figure 4 includes suggested attributions of the RA peaks with respect to participator (p) or spectator (s) states. Peaks marked with x cannot be assigned to either state with sufficient certainty. The participator states are similar to those formed upon direct valence ionization since the latter are also predominantly of 1h configuration. Hence, peaks associated with the participator states are present both in the RA spectra and the VUV PES. Below we motivate our assignments in Fig. 4, starting with the participator states, followed by the spectator states.

All RA spectra in Fig. 4 display a feature, p1, that matches the position (11.4 eV) of the lowest binding energy (BE) peak of the VUV PES. It is therefore, as mentioned earlier, assigned to a participator state associated with ejection of the electron from the $13a'$, $12a'$ and $3a''$ orbitals (see Table I). Another band, x1, appears at 13 eV at both the 1st (401.0 eV) and 2nd (402.3 eV) resonance of the N 1s-edge RA spectra. We assign it to parent-ion vibrational excitation connected with p1 since there is no $1h$ or $2h-1p$ state predicted by theory or observed in the VUV PES at this BE (see Table I). A similar observation of a small band close to the lowest-energy RA peak was observed in the RA spectra of FNMA, which was interpreted in the same way[34].

In previous studies[40,41] a photoelectron band observed at 13.8 eV, similar to that discovered in our VUV PES (see Fig. 1), was tentatively assigned in Ref.[40] to a diexcited state of

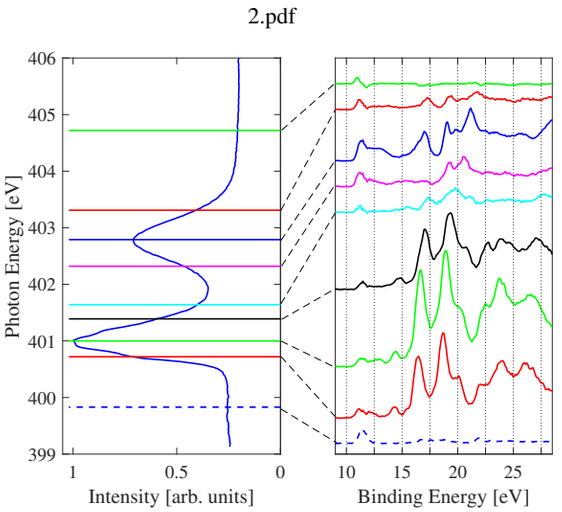

FIG. 2. RA spectra (right panel) recorded at the excitation energies indicated by the horizontal lines in the NEXAFS spectrum (left panel) at the N 1*s*-edge. The NEXAFS peaks at 401.0 eV and 402.3 eV represent excitations to the LUMO and LUMO+1 orbitals, respectively. The below-resonance contribution recorded at 399.8 eV excitation energy (dashed blue line in the right panel) has been subtracted from the RA spectra. The experimental energy resolution is ∼200 meV for the NEXAFS spectrum and ∼700 meV for the RA spectra.

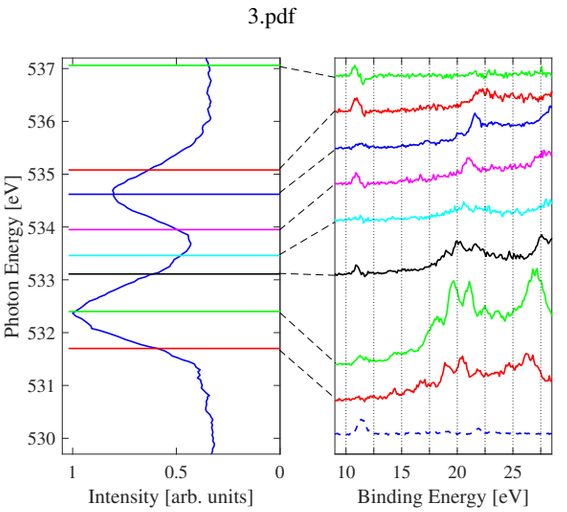

FIG. 3. Same as Fig. 2, but for the O 1*s*-edge. The NEXAFS peaks at 532.4 eV and 534.6 eV represent excitations to the LUMO and LUMO+1 orbitals, respectively. The below-resonance contribution (dashed blue line in the right panel) is recorded at 525.5 eV excitation energy. The experimental energy resolution is ∼300 meV for the NEXAFS spectrum and ∼850 meV for the RA spectra.

ClNO. However, our data suggests that the peak at 13.8 eV originates from NO. Moreover, we do not observe any corresponding RA feature at this BE, for any of the resonant excitations, which would be expected if it was a diexcited state.

The two pronounced peaks at 17.2 eV and 19.0 eV in the VUV PES have participator counterparts (p2 and p3) at matching positions in the RA spectrum recorded with 402.3 eV photon energy. They are also evident in the spectrum produced upon 401.0 eV excitation, but in this case the p2-peak overlaps with the contribution from residual N_2. Indeed, this BE roughly coincides with that of the N 1*s* electron in N_2[49]. The residual N_2 contributions appear only in the 401.0 eV RA spectrum. Their positions match those of the two main features of the pure N_2 spectrum[49], at 16.7 eV and 23.7 eV, according to our photoelectron-ion coincidence measurements presented in section III C (see Fig. 5(b)). Weak signatures of p2 and p3 are also observed upon 534.6 eV excitation.

The VUV PES displays two peaks at 22.1 eV and 23.1 eV and their counterparts in the RA spectra appearing at the 1st resonance of the N 1*s*- and O 1*s*-edges are denoted as p4 and p5. At the N 1*s* resonance the p5-peak is, however, not directly visible since it overlaps with the N_2 feature.

The spectator states are assigned in the RA spectrum based on the assumption that they will have insignificant contributions in the VUV spectrum. Apparently this assumption is not strictly valid for the case of the complete breakdown of the molecular orbital picture of ionization when shake-up states can have intensities comparable to main lines. As discussed earlier, this phenomenon can be relevant for the VUV spectrum above 23 eV.

The first potential spectator state, s1, is observed at 14.5 eV in the RA spectra recorded at the 1st resonance of the N 1*s*- (401.0 eV) and O 1*s*-edge (532.4 eV). These peaks match quite well the calculated IEs (14.54 eV and 14.93 eV) of the diexcited ($2h-1p$) states. The assignment to a spectator state is also supported by the appearance of the peaks only at the 1st resonance of the two edges. A spectator state corresponding to the same two-hole configuration, but upon excitation to the 2nd resonance, would be shifted towards higher BEs.

The peaks at 18.2 eV (s2) and 21.1 eV (s4) of the 532.4 eV RA spectrum are also assigned to spectator states since there are no matching VUV-PES features. However, x2, between them, cannot be confidently assigned to either a participator or a spectator state. It may have contributions both from p3 and a spectator state.

Two peaks, assigned s3 and s5, appear at similar positions (20.0 eV and 21.4 eV) in the RA spectra recorded at the 2nd resonances of the N 1*s*- and O 1*s*-edge. Since both s3 and s5 are located where there is no VUV-PES peak, we attribute them to spectator states. Another peak, x3, emerges as a shoulder to p3 in the RA spectrum measured at the 1st resonance of the N 1*s*-edge. It is located at a similar position as s3 but it can not be the same state since it is associated with the 1st resonance and would, if that was the case, shift towards lower BEs. Instead x3 may be a vibrational shoulder connected with the p3 main peak.

The broad bands at ∼27 eV (s6) for the 1st resonances of the N 1*s*- and O 1*s*-edge, and at ∼29 eV (s7) for the 2nd resonances, are attributed predominantly to spectator states. The correlation of the band positions with the resonance excited, i.e., the shift of the bands to higher BEs upon excitation to the

4.pdf

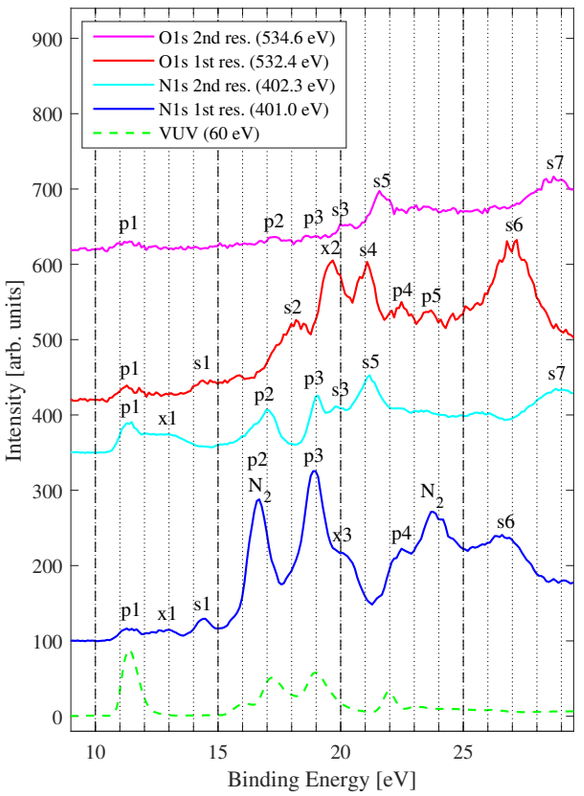

FIG. 4. RA spectra recorded upon excitation at the 1st (blue) and 2nd (cyan) N 1*s*-edge resonances, and the 1st (red) and 2nd (magenta) O 1*s*-edge resonances. The VUV PES is displayed with a dashed green line. The assignments of the peaks are indicated by the letters p, for participator state, s, for spectator state, and x, for uncertain attributions. N_2 indicates peaks influenced by N_2 contribution. The experimental energy resolutions of the VUV PES and the RA spectra for the N 1*s*- and O 1*s*-edges are specified in the figure captions of Figs. 1, 2 and 3, respectively.

2nd resonance, fits the behavior of spectator states.

We note that the RA spectra differ significantly between the resonances. For instance, the p2 and p3-peaks in Fig. 4 are highly pronounced only for the 401.0 eV resonance. The variation of the RA spectra for all different resonances shows that the population of states upon RA is very sensitive both to the core-site excited (N or O) and to the state that the core electron is excited to (LUMO or LUMO+1). The probability of Auger decay is related to the spatial overlap between the 1*s* orbital of the core-excited site, the excited-electron orbital (LUMO or LUMO+1) and the 1*h* orbital created after Auger decay[27,28]. Thus, the strong variation of the RA spectra with different excitations observed in Fig. 4 reflects the distinct electron-density distributions of, not just the 1*s* orbitals, which are located at different molecular sites, but also the LUMO and LUMO+1 orbitals, and it demonstrates the capability of RA spectroscopy to resolve them.

In Figs. 2 and 3 a gradual shift of the RA peaks towards higher BE with increasing photon energy close to a specific resonance, can be observed. This suggests that the higher vibrational excitation created by the increased photon energy partly stays in the produced parent ion, i.e., it is not transferred to the kinetic energy of the ejected electron, and consequently the measured BE grows.

C. Photoelectron-ion coincidence spectra

The photoelectron-ion coincidence measurements provide information about the produced fragment-ion yields connected with the RA spectral features. Figures 5(a)-5(e) show the yield of the main ion fragments (see legend) detected in coincidence with the electrons (red dashed line). The black dashed line represents the sum of all displayed ions. The spectra were recorded at the photon energies indicated in each figure. In Figs. 5(f)-5(j) the corresponding branching fractions, i.e., the relative yield of a fragment ion normalized to the sum of all ions, are presented. By normalizing with the sum of all ions, the relative yields are obtained with the influence from the electronic state emphasized. Consequently, the branching fraction is the relevant parameter for monitoring the effect of the electronic state formed upon Auger decay on the dissociation.

TABLE II. Calculated thermodynamic thresholds and experimental appearance energies upon VUV ionization for the fragmentation channels associated with the production of the specific ion fragments. The appearance energies are determined as the first point where the signal appears. A minimum error margin of ±0.2 eV is estimated based on the width (2σ) of the VUV-PES peaks. The values in square brackets represent the thermodynamic thresholds of the cationic three-body dissociation channels producing Cl^+ and O^+ respectively.

Ion fragment	Thermodynamic threshold (eV)	Experimental appearance energy (eV)
NO^+	10.85	11.0
Cl^+	14.53 [21.03]	14.6
ClN^+	16.23	17.2
O^+	20.35 [21.67]	20.3
N^+	22.67	22.9

Table II lists the calculated thermodynamic thresholds together with the experimental appearance energies extracted from the VUV photoelectron-ion coincidence spectra. In Figs. 5(a) and 5(f) the calculated thermodynamic thresholds of each fragment ion is marked with a vertical solid line following the color coding of the legend. Figure 5(f) shows that the appearance of each ion fragment matches quite well with the calculated thermodynamic thresholds upon VUV excitation, and this is true for the RA spectra as well.

Figure 5(f) shows that NO^+ (green line) is the only fragment ion produced below 13 eV. This observation is in line with our calculations of the thermodynamic thresholds (Table II) that imply that below 14.53 eV NO^+ is the only energet-

ically allowed fragment. When Cl^+ (blue line) appears the NO^+ fragment is suppressed. Both fragment ions are formed via two-body dissociation. NO^+ reappears at approximately 17.4 eV simultaneously with the rise of the PES-peak at 19.0 eV. It is clear from Fig. 5(f) that Cl^+ and NO^+ are preferentially formed at separate peaks, the 17.2 eV and the 19.0 eV PES-peaks, respectively. Specifically, the reappearance of NO^+ at the 19.0 eV peak cannot be explained with the opening of a new channel, that might be thermodynamically favored, but must be caused by the electronic state influence. In other words, the excess energy has not been significantly distributed in the molecule before the fragmentation. NO^+ is then suppressed along with the appearance of an additional Cl^+ channel at 21.5 eV, which produces three fragments, i.e., $Cl^+ + N + O$, and has a calculated thermodynamic threshold of 21.03 eV.

A small increase of ClN^+ (brown line) can be observed at the vibrational tail of the 17.2 eV PES-peak, which drops rapidly with the emergence of the 19.0 eV PES-peak and then appears again at the vibrational tail of the latter peak. It suggests that the formation of ClN^+ requires a high vibrational excitation of the parent ion at this BE-region. A similar behavior is demonstrated for the corresponding participator peaks in the RA spectra [see Figs. 5(g),(h) and (j)]. An analysis of the vibrational tail of the two peaks reveals that they have a strong contribution from the ClN-O stretching mode[29], which supports the above interpretation. The described sharp drop of the ClN^+ branching fraction precisely at the onset of the 19.0 eV PES-peak is another strong indication of the fragmentation being influenced by the created state of the parent ion. Although in this case it relates to the vibrational state rather than the electronic state.

Above 20 eV the emergence of the N^+ (magenta line) and O^+ (black line) channels can be observed. The N^+ branching ratio (and also the absolute yield) then drops sharply at 29.2 eV while Cl^+ and NO^+ increases. This can be interpreted as the opening of the doubly charged fragmentation channels. Since the doubly charged fragmentation channels involving N^+ are predicted to open at higher BEs, ∼35.5 eV according to our calculations, N^+ is not produced when the parent ions become doubly charged, which results in the reduction of N^+. Instead the first doubly charged fragmentation channel, $ClNO^{2+} \rightarrow Cl^+ + NO^+$, increases. The observed appearance of the doubly charged fragmentation channel at approximately 29.2 eV is in line with the results from double-photoionization measurements of ClNO performed by members of our research group. These data suggest that the appearance energy of the $Cl^+ + NO^+$ channel is 30.08 eV[50].

Figures 5(f)-(j) display similar branching fractions for the VUV excitation and all resonances, except for that associated with the first resonance of the O 1*s*-edge in Fig. 5(i). The latter stands out by having a significantly increased ClN^+ branching fraction compared with the other resonances. From Fig. 5(i) it follows that the increase in ClN^+ is strongly connected with the peaks labeled s2 and s4, at 18.2 eV and 21.1 eV, respectively. Peaks s2 and s4 are attributed to spectator states formed by excitation to the LUMO orbital, which is of NO antibonding character. It suggests that the formation of a spectator state with an excited-electron orbital characterized by NO-bond weakening, favors the production of ClN^+ fragments, which are produced by breaking the NO bond. It shows again that the character of a specific state can have a significant effect on the branching fraction, and thus on the relative yields of produced fragments. In Ref.[19] the relative yield of ClN^+ at the 1st resonance of the O 1*s*-edge was measured to be 8.1% compared with 1.4% at the 2nd resonance, when producing single ions. This difference can be explained, in view of the present results, by the influence of the spectator states s2 and s4.

The correlation between the electronic character and the fragmentation products demonstrated in the present study of ClNO was not observed in our previous investigation of FNMA[34]. Instead, the excess energy of the FNMA molecule upon formation of a specific state seemed to be the dominating factor for the branching fractions. The difference may be related to the size of the two molecules, i.e., for smaller molecules the character of the states more strongly influences the branching fractions of the formed ion fragments. For a small molecule like ClNO, the potentially slow energy redistribution, based on Fermi's golden rule arguments, allows the character of the Auger state to influence the fragmentation process. It prevents the electronic character to be washed out by the redistribution of the electronic energy into vibrational energy. We note that for doubly, or higher, charged parent ions formed by direct core ionization, the situation can be similar since the fragmentation may occur quickly via Coulomb explosion[21], and thus precede the energy-redistribution.

In contrast to the 1st resonance of the O 1*s*-edge, the corresponding excitation at the N 1*s*-edge does not result in a similar increase in ClN^+ branching fraction. This is observed in Fig. 5(b) and 5(g), which show the relative yields and branching fractions, respectively. It is also supported by the measured relative yields of ClN^+ in Ref.[19], which show just a slightly enhanced ClN^+ yield at the 1st resonance of the N 1*s*-edge (3.5%) compared with the 2nd resonance (2.6%). Hence, there is also a site-specific effect on the fragmentation, i.e., the core-excited site influences the branching fractions and relative yields of the formed fragments. In the present case core-excitation at the O-site leads to preferential breaking of the nearest bond, the NO bond, favoring the formation of ClN^+, while core-excitation at the N-site tends to break both neighboring bonds, the NO and the ClN bonds, which results in a reduced ClN^+ yield compared with the core-excitation at the O-site. The observed site-specific difference is connected with the different cross-section for creating the s2 and s4 states upon excitation. This is, in turn, connected with the overlap of the orbitals involved in the Auger process, as mentioned above, and it suggests that the orbitals of the holes associated with the s2 and s4 states have a stronger overlap with the O-site compared with the N-site.

IV. CONCLUSIONS

We have investigated the influence of the electronic states formed upon direct ionization and RA decay of ClNO, on

the fragmentation pattern. To this end we have measured the electron-ion coincidence spectra following VUV and resonant-core excitation at the N 1*s*- and O 1*s*-edges of the molecule. Also, a detailed analysis and assignment of features of the VUV PES and RA spectra are presented, which is central for extracting appropriate conclusions from the coincidence spectra regarding the role played by the final electronic states on the fragmentation. The extent of the electronic-state involvement addressed in this study is relevant for the possibility of selective bond breaking.

Although signatures of selective bond breaking have been observed previously upon valence and core ionization of molecules, explicit demonstrations are missing to verify the electronic-state influence on the fragmentation. Typically the measured relative fragment yields associated with a specific excitation, or with the ejected-electron binding energy corresponding to the formation of a particular electronic state, serve as an indirect indication of such influence. However, it is often difficult to conclude whether it is the final electronic state or the distributed excess energy of the parent ion that determines which bonds are broken. Here we explicitly demonstrate the influence of the electronic states formed upon direct VUV ionization or via RA decay, on the fragmentation of ClNO. It is revealed by two observations 1) a significantly increased formation of ClN^+ connected with two pronounced and well resolved spectator-state peaks, which is clearly distinguishable from the ion yields produced by the participator states. Notably, the spectator-electron orbital is anti-bonding at the NO bond for the spectator states, which suggests influence from this orbital character on the fragmentation. 2) A correlation between the formation of Cl^+ and NO^+ fragments with individual VUV-PES peaks, which is reproduced at the corresponding RA participator peaks. Importantly, the correlation can not be explained by the opening of a new fragmentation channel. We also show that the ClN-O vibrational-stretch excitation observed as vibrational tails of specific peaks is connected with the enhanced production of ClN^+ ions. It is an additional indication that the character of the formed state, and not the excess energy associated with them, determines the fragmentation branching fractions (at least below binding energies of 20 eV).

The electronic-state influence observed in the present study can to some extent be explained by the relatively small size of ClNO. For such small molecules the redistribution of the excess energy associated with the final electronic states can be slow according to Fermi's golden rule[30]. Consequently these electronic states have time to affect the fragmentation before the redistribution of excess energy in the molecule removes its influence. In contrast, the excess energy has been shown to play a critical role in similar studies of several larger molecules[9,26,34,51]. We note, however, that the redistribution rate can in general also depend on other properties than the size of the individual molecule.

ACKNOWLEDGMENTS

We acknowledge Elettra Sincrotrone Trieste for providing access to its synchrotron radiation facilities. Calculations were performed on resources at the Chalmers Centre for Computational Science and Engineering (C3SE) provided by the Swedish National Infrastructure for Computing (SNIC). The authors also acknowledge the open access contribution of the Research Infrastructure (RI) Elettra.

DATA AVAILABILITY STATEMENT

The data that support the findings of this study are available from the corresponding author upon reasonable request.

V. REFERENCES

[1] X. Wang et al., Phys. Chem. Chem. Phys. **23**, 11900 (2021).
[2] W. Eberhardt, T.K. Sham, R. Carr, S. Krummacher, M. Strongin, S. L. Weng, and D. Wesner, Phys. Rev. Lett. **50**, 1038 (1983).
[3] P. Salen, V. Yatsyna, L. Schio, R. Feifel, R. Richter, M. Alagia, S. Stranges, and V. Zhaunerchyk, J. Chem. Phys. **144**, 244310 (2016).
[4] J. H. D. Eland, P. Linusson, M. Mucke, and R. Feifel, Chem. Phys. Lett. **548**, 90 (2012).
[5] S. Zagorodskikh, J. H. D. Eland, V. Zhaunerchyk, M. Mucke, R. J. Squibb, P. Linusson, and R. Feifel, J. Chem. Phys. **145**, 124302 (2016).
[6] Y.-T. Wang, Y.-J. Chiang, and C.-L. Liu, Chem. Phys. Lett. **759**, 137967 (2020).
[7] M. C. Nelson, J. Murakami, S. L. Anderson, and D. M. Hanson, J. Chem. Phys. **86**, 4442 (1987).
[8] S. Nagaoka, H. Fukuzawa, G. Prümper, M. Takemoto, O. Takahashi, K. Yamaguchi, T. Kakiuchi, K. Tabayashi, I. H. Suzuki, J. R. Harries, Y. Tamenori, and K. Ueda, J. Phys. Chem. A **115**, 8822 (2011).
[9] H. Levola, E. Itälä, K. Schlesier, K. Kooser, S. Laine, J. Laksman, D. T. Ha, E. Rachlew, M. Tarkanovskaja, K. Tanzer, and E. Kukk, Phys. Rev. A - At. Mol. Opt. Phys. **92**, 063409 (2015).
[10] C. Miron, M. Simon, N. Leclercq, D.L. Hansen, and P. Morin, Phys. Rev. Lett. **81**, 4104 (1998).
[11] A. Naves de Brito, S. Sundin, R.R. Marinho, I. Hjelte, G. Fraguas, T. Gejo, N. Kosugi, S. Sorensen, and O. Björneholm, Chem. Phys. Lett. **328**, 177–187 (2000).
[12] P. Bolognesi, J. A. Kettunen, A. Cartoni, R. Richter, S. Tosic, S. Maclot, P. Rousseau, R. Delaunay, and L. Avaldi, Phys. Chem. Chem. Phys. **17**, 24063 (2015).
[13] J. H. D. Eland, S. Zagorodskikh, R. J. Squibb, M. Mucke, S. L. Sorensen, and R. Feifel, J. Chem. Phys. **140**, 184305 (2014).
[14] P. Salen, M. Kaminska, R.J. Squibb, R. Richter, M. Alagia, S. Stranges, P. van der Meulen, J.H.D. Eland, R. Feifel and V. Zhaunerchyk, Phys. Chem. Chem. Phys. **16**, 15231 (2014).
[15] S. Nagaoka et al., Phys. Rev. A **75**, 020502(R) (2007).
[16] L. Schwob et al., J. Phys. Chem. Lett. **11**, 1215 (2020).
[17] M. Gerlach et al., J. Chem. Phys. **154**, 114302 (2021).
[18] W. Habenicht, H. Baiter, K. Muller-Dethlefs, and E. W. Schlag, Phys. Scr. **41**, 814-818 (1990).
[19] P. Salen, L. Schio, R. Richter, M. Alagia, S. Stranges, and V. Zhaunerchyk, J. Chem. Phys. **149**, 164305 (2018).
[20] L. J. Butler, E. J. Hintsa, S. F. Shane, and Y. T. Lee, J. Chem. Phys. **86**, 2051 (1987).
[21] L. Inhester, B. Oostenrijk, M. Patanen, E. Kokkonen, S. H. Southworth, C. Bostedt, O. Travnikova, T. Marchenko, S. K. Son, R. Santra, M. Simon, L. Young, and S. L. Sorensen, J. Phys. Chem. Lett. **9**, 1156 (2018).
[22] P. Salek et al., Phys. Rev. A **62**, 062506 (2000).

[23]E. Meneghin, C. Leonardo, A. Volpato, L. Bolzonello, and E. Collini, Sci. Rep. **7**, 11389 (2017).
[24]E. Kukk et al. Phys. Rev. Research **3**, 013221 (2021).
[25]E. P. Mansson S. De Camillis, M. C. Castrovilli, M. Galli, M. Nisoli, F. Calegari, and J. B. Greenwood, Phys. Chem. Chem. Phys. **19**, 19815 (2017).
[26]E. Kukk, D. T. Ha, Y. Wang, D. G. Piekarski, S. Diaz-Tendero, K. Kooser, E. Itälä, H. Levola, M. Alcami, E. Rachlew, and F. Martin, Phys. Rev. A - At. Mol. Opt. Phys. **91**, 043417 (2015).
[27]S. Stranges, M. Y. Adam, C. Cauletti, M. De Simone, C. Furlani, M. N. Piancastelli, P. Decleva, and A. Lisini, J. Chem. Phys. **97**, 4764 (1992).
[28]D. B. Thompson, D. Ji, S. Y. Chen, and D. M. Hanson, J. Phys. B At. Mol. Opt. Phys. **32**, 5711 (1999).
[29]M.I. Abbas, J.M. Dyke, and A. Morris, J. Chem. Soc., Faraday Trans. 2 **72**, 814 (1976).
[30]E. Fermi, Nuclear physics, University of Chicago Press, Ch. 8, p. 142 (1950).
[31]M.S Shuurman and A. Stolow, Annu. Rev. Phys. Chem. **69**, 427 (2018).
[32]G. G. Lehmann and G. Scoles, Annu. Rev. Phys. Chem. **45**, 241 (1994).
[33]T. S. Kuhlman, T. I. Solling, and K. B. Moller, ChemPhysChem. **13**, 820 – 827 (2012).
[34]P. Salen, L. Schio, R. Richter, M. Alagia, S. Stranges, and V. Zhaunerchyk, Phys. Rev. A **102**, 032817 (2020).
[35]L. Philava, J. Niskanen, K. Kooser, C. Strålhman, S. Maclot, A. Kivimäki, and E. Kukk, Phys. Chem. Chem. Phys. **23**, 21249 (2021).
[36]L. Schio *et al.*, Phys. Chem. Chem. Phys. **17**, 9040 (2015).
[37]R. R. Blyth, R. Delaunay, M. Zitnik, J. Krempasky, R. Krempaska, J. Slezak, K. C. Prince, R. Richter, M. Vondracek, R. Camilloni, L. Avaldi, M. Coreno, G. Stefani, C. Furlani, M. De Simone, S. Stranges, and M. Y. Adam, J. Electron Spectros. Relat. Phenomena **101–103**, 959 (1999).
[38]O. Plekan, M. Coreno, V. Feyer, A. Moise, R. Richter, M. De Simone, R. Sankari, and K. C. Prince, Phys. Scr. **78**, 058105 (2008).
[39]M. J. Frisch et al., Gaussian 16, Revision B.0, Gaussian, Inc., Wallingford CT, (2016).
[40]S. Lacombe, M. Loudet, A. Dargelos, and J.M. Camou, Chem. Phys. **258**, 1-12 (2000).
[41]D.C. Frost, S.T. Lee, C.A. McDowell, and N.P.C. Westwood, J. Electron Spectrosc. Rel. Phenom. **7**, 331 (1975).
[42]M.S. Deleuze and L.S. Cederbaum, J. Chem. Phys., **105 (17)**, 7583 (1996).
[43]G. Öhrwall et al., J. Chem. Phys. **123**, 054310 (2005).
[44]H. Brion, C. Moser, and M. Yamazaki, J. Chem. Phys. **30**, 673 (1959).
[45]V. Kumar, Thesis (1969).
[46]O. Edqvist, L. Åsbrink, and E. Lindholm, Z. Naturforsch. **26a**, 1407—1410 (1971).
[47]R. Fantoni, A. Giardini-Guirdoni, and R. Tribelli, J. Electron Spectrosc. Rel. Phenom., **26**, 99-105 (1982).
[48]P. Baltzer, M. Larsson, L. Karlsson, B. Wannberg, and M. Carlsson Göthe, Phys. Rev. A, **46 (9)**, 5545 (1992).
[49]D. Ceolin, C. Miron, M. Simon, and P. Morin, J. Electron Spectrosc. Rel. Phenom. **141**, 171-181 (2004).
[50]Double photoionization of nitrosyl chloride by synchrotron radiation in the 24-70 eV photon energy range, submitted manuscript.
[51]S. Sen et al., Phys. Chem. Chem. Phys. **24**, 2944 (2022).

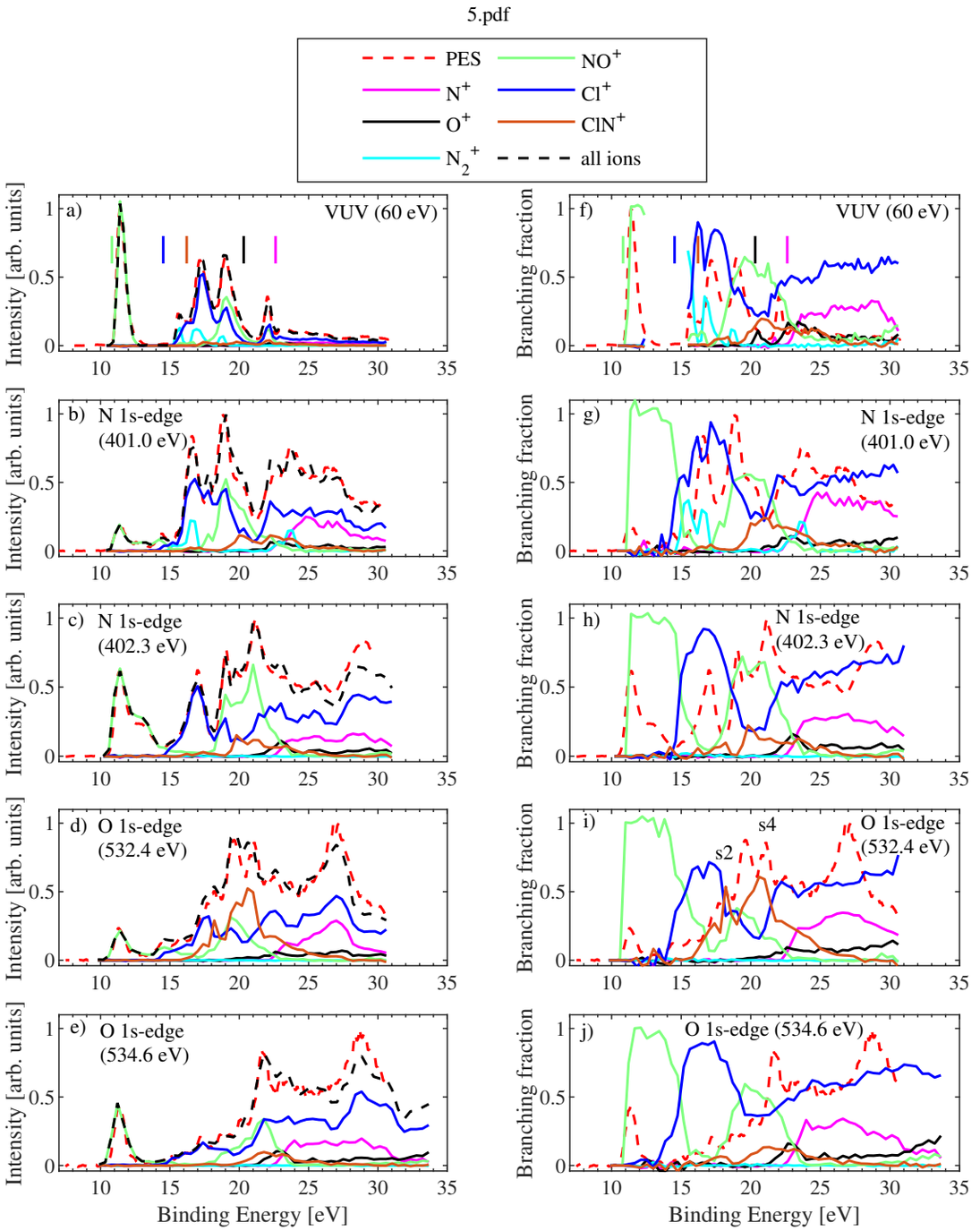

FIG. 5. Plots showing the electron spectra (red dashed) of ClNO and the intensities (a-e) of fragment ions (see legend) in coincidence with the ejected electrons. The plots are presented for (a) VUV-excitation (60 eV) and for resonant excitations at the N 1*s*-edge [(b) 401.0 eV, (c) 402.3 eV], and at the O 1*s*-edge [(d) 532.4 eV, (e) 534.6 eV]. Figures 5(f)-(j) display the corresponding branching fractions, i.e., the yield of each fragment normalized to the total ion yield of all presented fragments. Below-resonance contributions have not been removed in any of the plots. The calculated thermodynamic thresholds of each fragment ion are marked with vertical lines and with colors indicated in the legend. In panel (i), two PES peaks, s2 and s4, assigned to spectator states are indicated. They are discussed more in the text. The VUV branching fractions have been omitted in the region of BE = 12.4−15.5 eV in panel (f) due to the limited signal resulting from a low cross-section for the photo-electron process. The experimental energy resolutions of the electron spectra and the electron-ion coincidence spectra are ∼400 meV (VUV-excitation), ∼700 meV (N 1*s*-edge) and ∼850 meV (O 1*s*-edge).

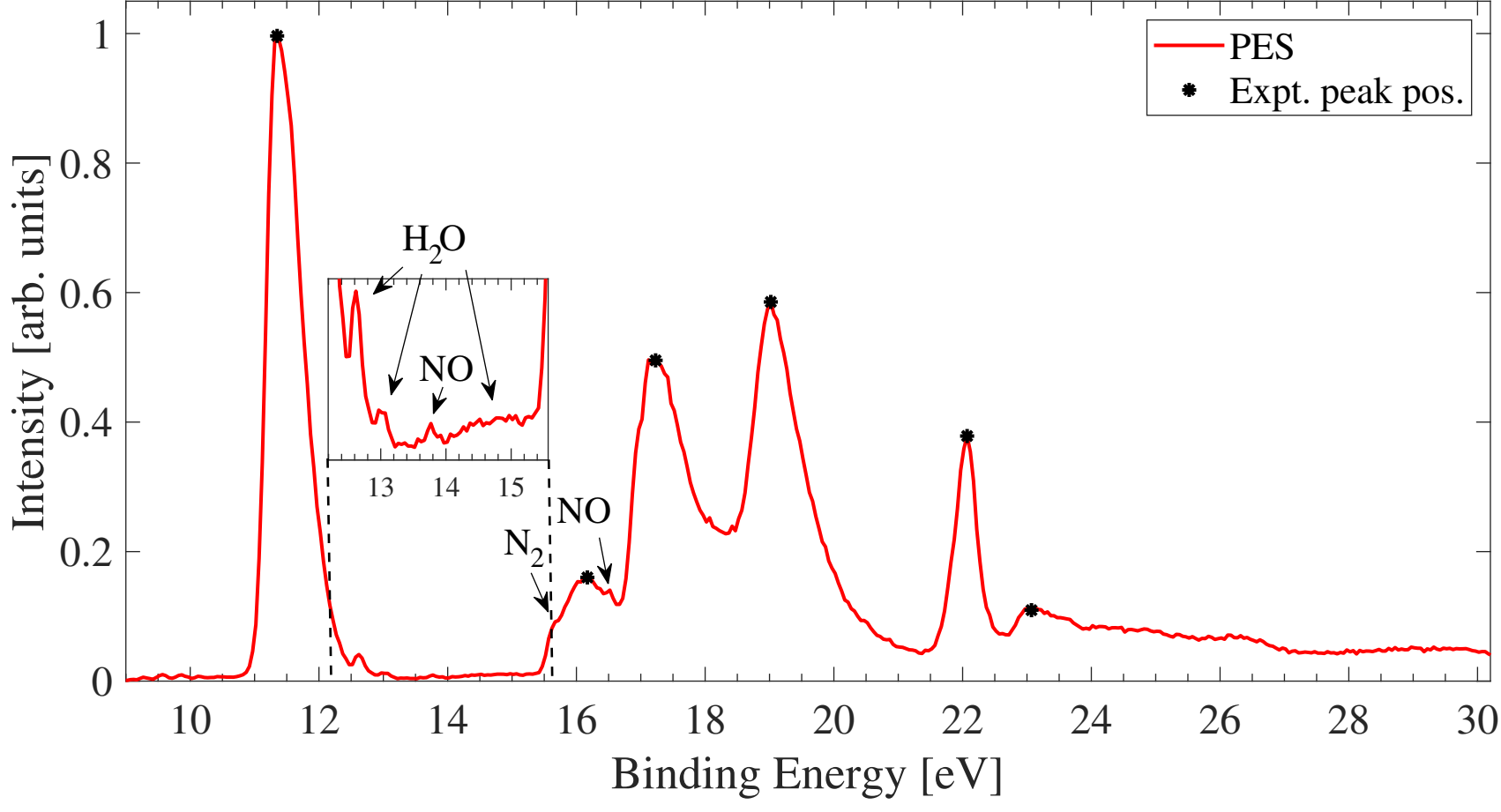
PES
Expt. peak pos.
Intensity [arb. units]
Binding Energy [eV]
H2O
NO
N2
NO
0
0.2
0.4
0.6
0.8
1
10
12
14
16
18
20
22
24
26
28
30
13
14
15

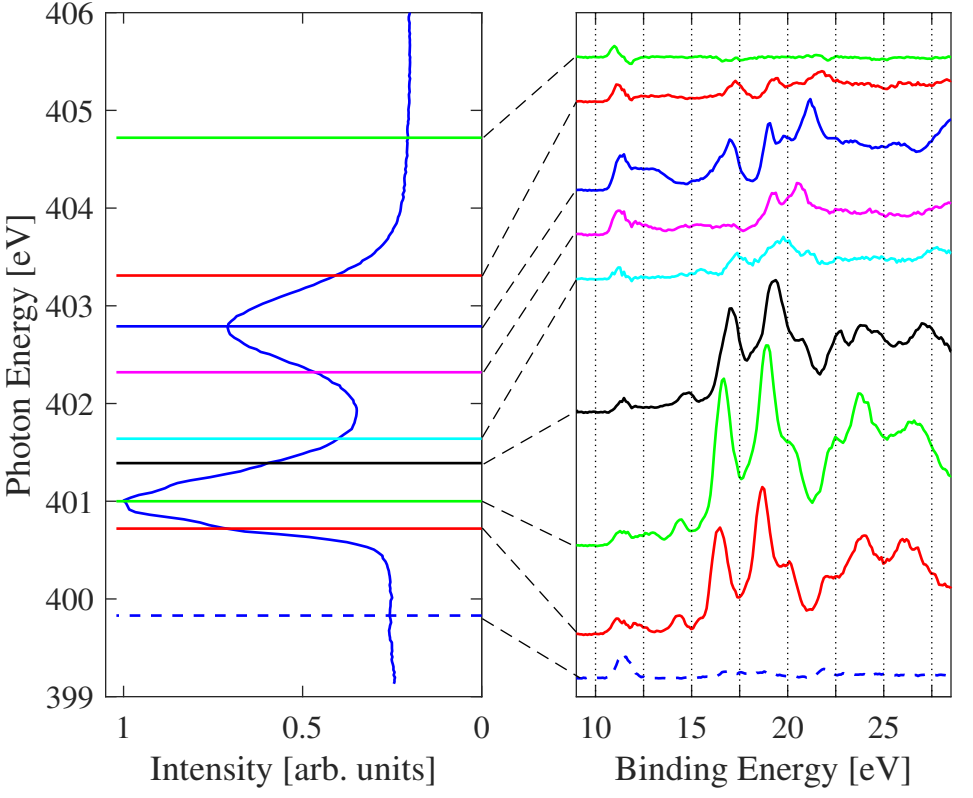
406
405
404
403
402
401
400
399
Photon Energy [eV]
1
0.5
0
Intensity [arb. units]
10
15
20
25
Binding Energy [eV]

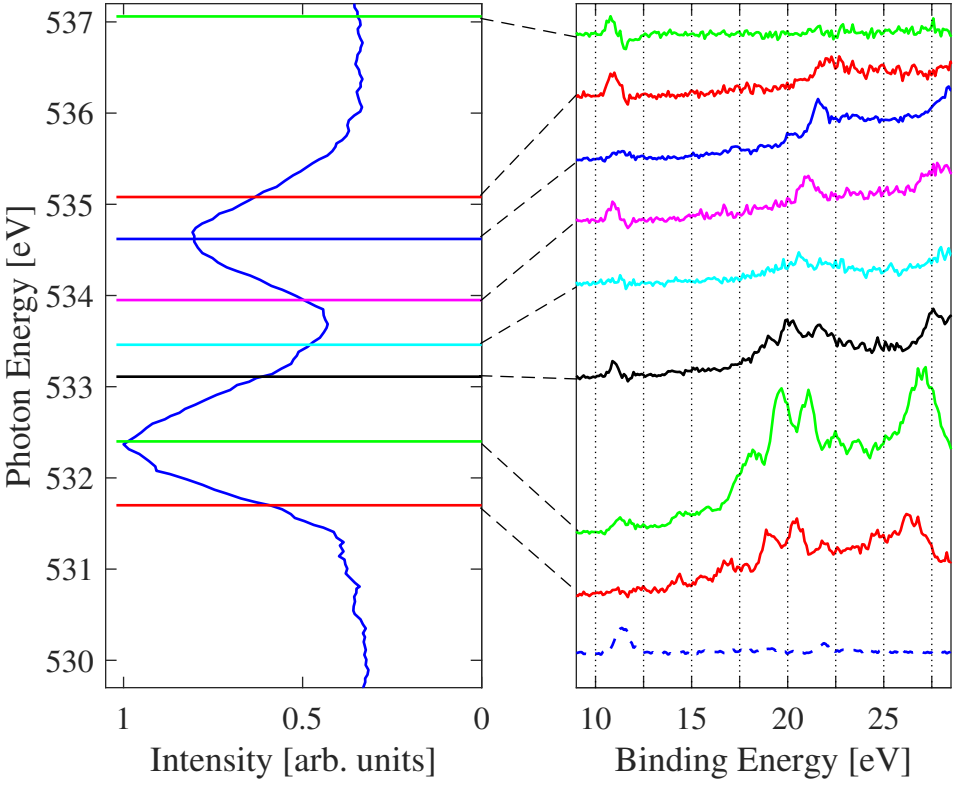
Photon Energy [eV]
537
536
535
534
533
532
531
530
1
0.5
0
Intensity [arb. units]
10
15
20
25
Binding Energy [eV]

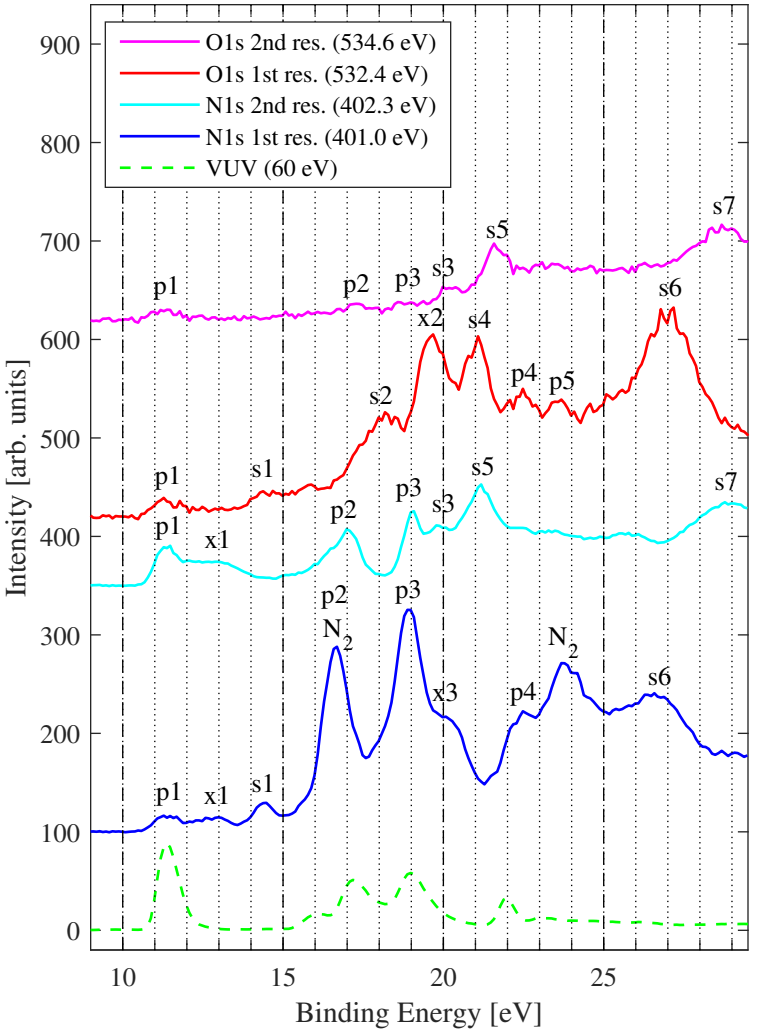
O1s 2nd res. (534.6 eV)
O1s 1st res. (532.4 eV)
N1s 2nd res. (402.3 eV)
N1s 1st res. (401.0 eV)
VUV (60 eV)
Intensity [arb. units]
Binding Energy [eV]
900
800
700
600
500
400
300
200
100
0
10
15
20
25
p1
p2
p3
s3
s5
s7
x2
s4
s6
p4
p5
s2
p1
s1
p1
x1
p2
p3
s3
s5
s7
p1
x1
s1
p2
N2
p3
x3
p4
N2
s6

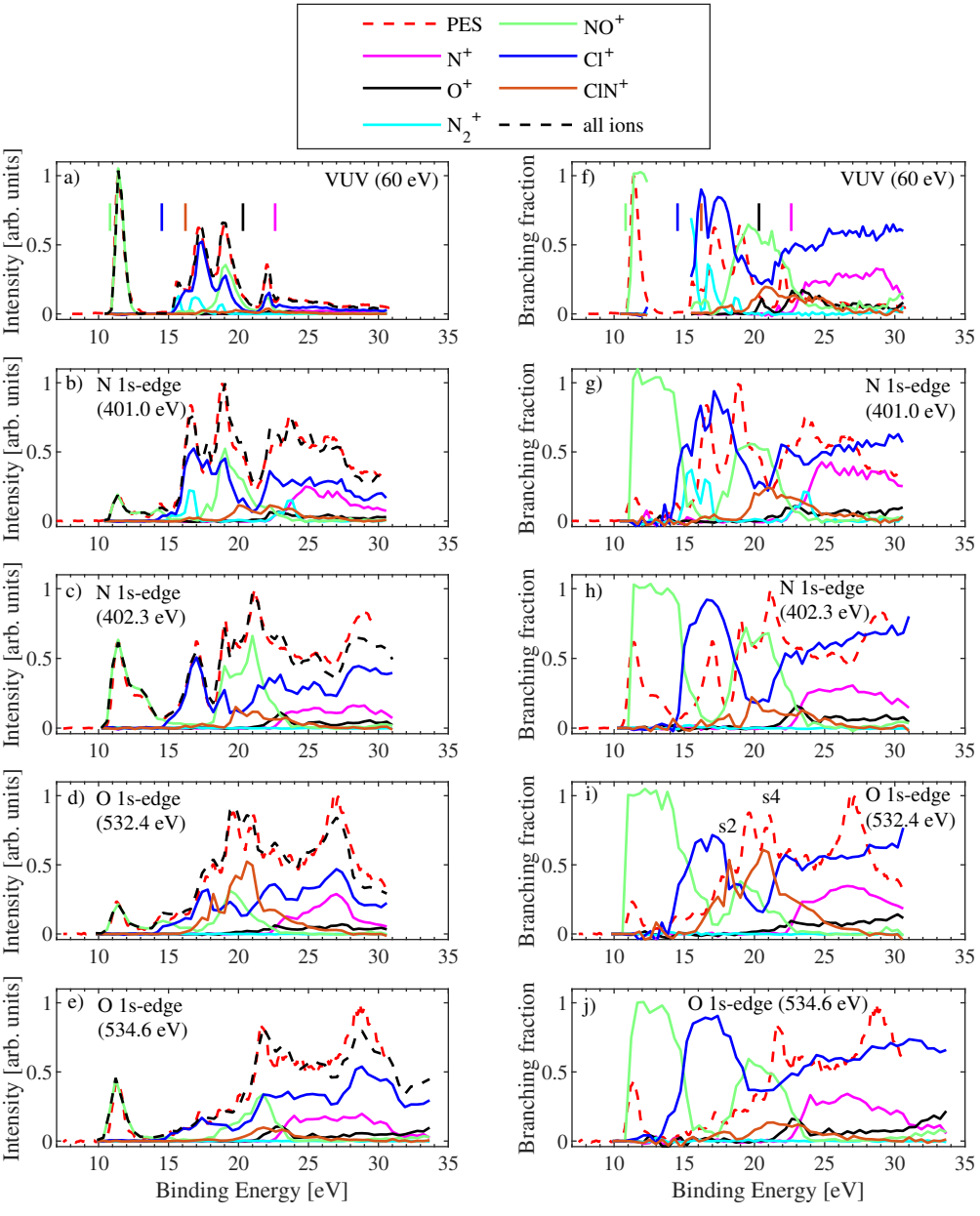
PES
NO+
N+
Cl+
O+
ClN+
N2+
all ions
a)
VUV (60 eV)
b) N 1s-edge (401.0 eV)
c) N 1s-edge (402.3 eV)
d) O 1s-edge (532.4 eV)
e) O 1s-edge (534.6 eV)
f)
VUV (60 eV)
g)
N 1s-edge (401.0 eV)
h)
N 1s-edge (402.3 eV)
i)
s4
s2
O 1s-edge (532.4 eV)
j)
O 1s-edge (534.6 eV)
Intensity [arb. units]
Branching fraction
Binding Energy [eV]